Perpendicular Domain Orientation in Dense Planar Brushes of Diblock Copolymers

ARTICLE *in* MACROMOLECULES · JUNE 2012

Impact Factor: 5.8 · DOI: 10.1021/ma300890w

Macromolecules

Article

pubs.acs.org/Macromolecules

Perpendicular Domain Orientation in Dense Planar Brushes of Diblock Copolymers

Andrey A. Rudov,[†] Pavel G. Khalatur,[‡] and Igor I. Potemkin*[,†,‡]

[†]Physics Department, Moscow State University, Moscow 119991, Russian Federation

[‡]Institute for Advanced Energy Related Nanomaterials, Ulm D-89069, Germany

ABSTRACT: Dense planar brushes of diblock copolymers physically attached to the substrate by end groups are studied by the dissipative particle dynamics simulation technique. We predict stability of spatially ordered perpendicularly oriented domains which are separated from the substrate and the free surface of the film by homogeneous layers of different type. Depending on composition of the copolymer, various structures including hexagonally ordered "golf holes", parallel "gullies" and "ridges", and "stalactites" ordered with the symmetry of hexagonal lattice can be stable. We analyze regimes of good and poor solvents for both blocks (nonselective solvents). Physical reasons for perpendicular domain orientation are discussed. In the case of low "grafting" density, our results coincide with those reported in the literature.

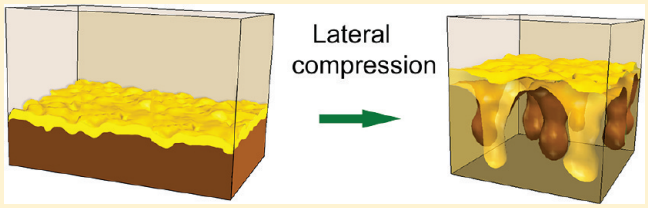

INTRODUCTION

The problem of perpendicular orientation of nanodomains in block copolymer films has been attracting considerable attention due to high potential of such films for many applications including growth of ultrahigh-density nanowire arrays for storage media,[1] manufacturing of organic photovoltaic devices with developed interfacial area to efficiently perform charge collection and transfer to electrodes,[2] etc. There are few ways controlling nanodomain orientations. Equilibrium perpendicular orientation in diblock copolymer films is achieved if interactions of both blocks with the film surfaces are similar[3,4] (the so-called neutral surfaces). To obtain such similarity, the surfaces can be modified by random AB copolymer consisting of monomer units identical to the diblock copolymer ones.[5] The molecular weight of diblock copolymers can also be responsible for control of equilibrium orientations. For example, symmetric high-molecular-weight PS-*b*-PB diblock copolymer on silicon oxide substrate forms perpendicular lamellae, and short enough diblocks exhibit layered structure.[6,7] In the case of patterned substrates, selective interactions of A and B blocks with the patterns can promote perpendicular domain orientation, if the period of the pattern is conformed with the bulk period of the block copolymer.[8−11] Decoration of the diblock copolymers by mesogen side groups can also lead to perpendicular orientation of amorphous nanodomains.[12,13] Improvement of long-range order[1] or enforced domain orientation[14,15] can be done by electric field for copolymers differing in the dielectric constant of the blocks (the domains are oriented in the direction of the field[14,15]).

In this paper, we propose another way promoting perpendicular domain orientation in diblock copolymer films which is accompanied by formation of A and B boundary layers (Figure 1). Such microstructures are formed in dense brushes of diblock copolymers physically attached by one end to the flat surface. Despite a quite a number of publications on block copolymer brushes in a selective solvent[16−19] and free of the solvent,[20−22] this effect was either not detected because of relatively low grafting density (melt brushes[20−22]) or the authors predicted poorly ordered lateral structures because of effects of good solvent (swollen brushes) and random chemical grafting of the chains making the domains less pronounced.[19] For example, stability of different kinds of surface micelles of rarely grafted copolymers was predicted in ref 16 using the scaling approach and a lattice self-consistent field theory (SCFT). Considering melt brushes of the thickness on the order of the Gaussian size of the molecule (this particular case predefines low enough grafting density), a hexagonal array of hemispherical micelles, parallel hemispherical stripes, inverse micelles, and bilayer were calculated (SCFT) as stable structures in the case of equal interaction parameters of A and B species with the free surface.[20,21] Further coarse-grained DPD simulations confirmed stability of such morphologies.[22] Higher grafting densities of diblock copolymer brushes in selective solvents were considered in ref 19 using single-chain-in-mean-field simulations. It has been shown that in the case of good solvent for both blocks and high repulsion between A and B monomer units the flat A/B interface becomes unstable and the lateral structure in the local position of the A/B interface adopts elongated, wormlike shapes (the so-called ripple and dimple structures). Such structures are characterized by broad concentration profiles. In the case of poor solvent for both blocks (this regime is closer to the melt brushes), the ripple and dimple structures were less pronounced, probably due to lower grafting density of the chains in comparison with the case of cosolvent.[19]

Received: May 2, 2012
Published: May 15, 2012

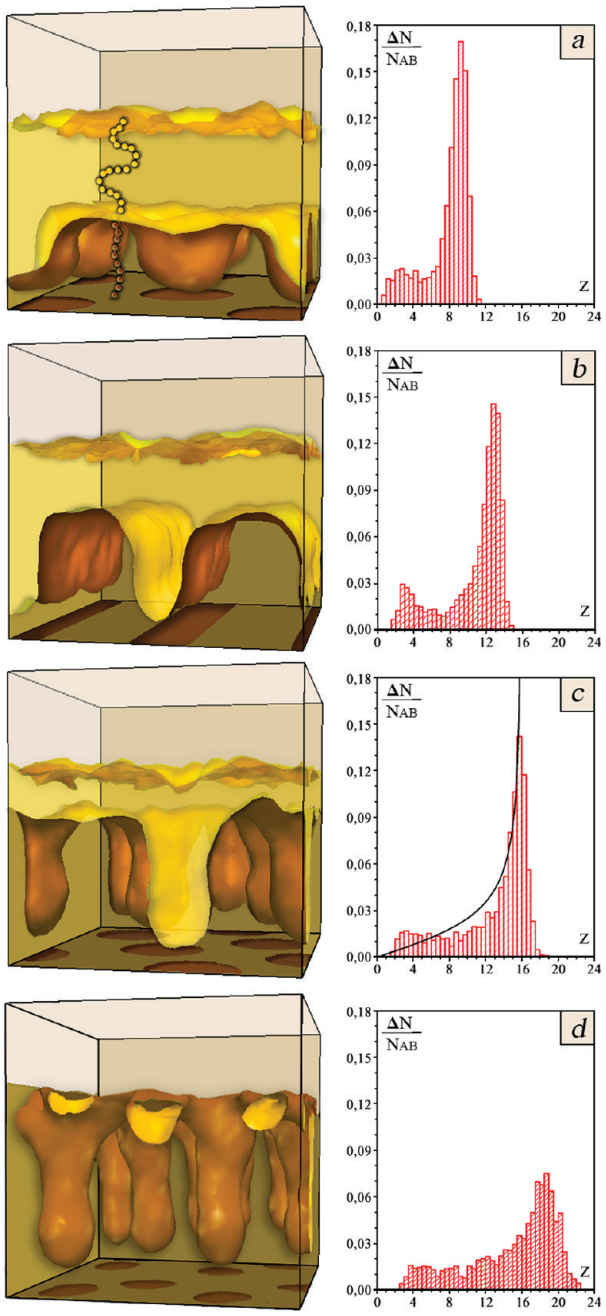

Figure 1. Possible structures of densely "end-grafted" diblock copolymer brushes (the end of A (brown) block is physically attached to the substrate and the end of B (yellow) block is free): hexagonally ordered "golf holes", 10_A-20_B (a); parallel "gullies" and "ridges", 14_A-16_B (b); hexagonally ordered "stalactites", 18_A-12_B (c) and 22_A-8_B (d). Brown disks and stripes on the substrate (bottom side of the box) depict projections ("shadows") of the corresponding domains. The surface "grafting" density $\sigma_S = 0.7$, $L_x = L_y = L_z = 32$, and the solvent is good for both blocks, $a_{AS} = a_{BS} = 25$. The fraction of AB junctions as a function of the distance z from the substrate for each of the structures is presented in the right column. Black solid line in the histogram c corresponds to the distribution function of chain ends in the case of homopolymer brush[27] of the thickness 16. For visual clarity, the solvent particles, which fully occupy the upper region (above upper yellow boundary) and partly the brush providing its swelling, are not shown.

In contrast with refs 19−22, we consider dense brushes of diblock copolymers *physically attached* to a plane surface by end groups of the chains (the end of A block is attached and the end of B block is free). Regimes of good and poor solvent for both blocks (nonselective solvent) are analyzed. The latter case approximately corresponds to the melt brushes: the poorer the solvent, the better the melt approximation.

SIMULATIONS

Our calculations are based on the dissipative particle dynamics (DPD) simulation technique.[23,24] The simulations are performed in a tetragonal box of constant volume $V = L_xL_yL_z$ ($L_x = L_y = L_z = 32$ and $L_x = L_y = 64$, $L_z = 32$) with a periodical boundary conditions in the x and y directions. All quantities are measured in units of the mass of the polymer bead, m_0, thermal energy, k_BT, and cutoff radius of the interaction potential, r_c. Thus, for the simplicity we will fix them as $m_0 = k_BT = r_c = 1$. Also, we set the total number density in the system as $\rho = N/V = 3$, so that the total number of the particles in the box is either $N = 3{\cdot}32^3$ ($L_x = L_y = 32$) or $N = 3{\cdot}32{\cdot}64^2$ ($L_x = L_y = 64$). There are four different types of the particles in the system: solvent particles (denoted by S), A- and B-beads forming copolymer brush, and the particles forming the walls at $z = 0$ and $z = L_z$ (labeled as W). The volume above the film is filled with single-site solvent particles (the initial structure before annealing of the system). The W-particles are arranged in such a way to form smooth, dense walls which prevent escape of all other particles from the system. We fix the total number of the beads in the chain as $n = 30$ and vary composition of the copolymer $f = n_A/n$ (the fraction of A units, i.e., the ratio of the number of A beads to the total number of the beads). Let us assume that the end-beads of the A blocks are physically attached to the wall at $z = 0$; i.e., they can freely migrate in the x−y plane, and their detachment from the wall is accompanied by the penalty in the energy of the system. The forces keeping the end beads near the wall and the beads in the chains are described by the Hook's law, $F^s_{ij} = -C_s(r_{ij} - r_{eq})$. Here the values of the spring constant $C_s = 4$ and $C_s = 5$ correspond to the bead−bead and bead−wall attraction, respectively, and the equilibrium distance between the attracting particles is $r_{eq} = 0$. We define the surface "grafting" density as $\sigma_s = N_{AB}/\rho^{2/3}L_xL_y$, where N_{AB} is the number of polymer chains in the box. The starting structures of the system before annealing correspond to complete separation of the polymer and solvent. Therefore, the brush swells during annealing. Furthermore, to prove convergency to the equilibrium structure, each time we prepare three different initial structures which relax to the single one during the annealing process. We confine ourselves by analysis of a nonselective solvent only; i.e., interactions of the solvent molecules with A and B species are quantified by equal parameters. The DPD method is based on the solution of the Newtonian equations of motion for all particles in the system. Each particle is subjected to the action of three different pairwise-additive forces: conservative, dissipative, and random ones. The conservative force is characterized by soft repulsion between nonbonded particles via the interaction parameters a_{ij}. The thorough set of the parameters is presented in Table 1. Inequality $a_{AA} = a_{BB} < a_{AB}$ means that A and B beads are incompatible even in the presence of the solvent. In general, one can estimate the Flory−Huggins parameters according to the formula[25] $\chi_{ij} = (0.286 \pm 0.002)(a_{ij} - a_{ii})$ at $\rho = 3$. Inequality $a_{AW} < a_{BW}$ means that repulsion of "nongrafted" B blocks from the substrate is higher than that of the attached A blocks. For nonselective solvent, $a_{AS} = a_{BS}$, and its quality is determined by absolute value of a_{AS}. In our calculations this parameter varies

dx.doi.org/10.1021/ma300890w | *Macromolecules* 2012, 45, 4870−4875

Table 1. DPD Interaction Parameters Used in Simulations[a]

a_{ij}	A	B	S	W
A	25	40	a_{AS}	25
B	40	25	a_{BS}	40
S	a_{AS}	a_{BS}	25	25
W	25	40	25	25

[a]The interaction parameters are represented in units of k_BT/r_c. The strength of AS and BS repulsions is varied (see the text).

in the interval between 25 and 35. a_{AS} = 25 corresponds to χ_{AS} = 0; the second virial coefficients for both blocks are positive and equal to 1/2 within the Flory–Huggins model. Therefore, we deal with a good solvent. If a_{AS} = 35 and χ_{AS} = 2.86, the second virial coefficient, $1/2 - \chi_{AS} = -2.36$, is negative, and the solvent is poor for both blocks. This regime corresponds approximately to the melt brushes. The dissipative and random forces are specified by the friction coefficients, γ_{ij}, and noise amplitudes, σ_{ij}, respectively, and play a role of the heat sink. The parameters γ_{ij} and σ_{ij} satisfy the fluctuation–dissipation theorem, $\sigma_{ij}^2 = 2\gamma_{ij}$, and in our simulations σ_{ij} is set to be 3. Finally, the equations of motion are integrated using a self-consistent leapfrog scheme[26] with a time step Δt = 0.05. The number of the time steps for equilibration of the system is 2×10^6 ($L_x = L_y = 32$) and 1×10^6 ($L_x = L_y = 64$).

RESULTS AND DISCUSSION

Depending on composition of the diblock copolymer, we predict stability of three kinds of "nontrivial" structures. Relatively short attached A blocks (10 beads) and long B blocks (20 beads) form partially interpenetrating bilayer. The region of interpenetration represents hexagonally arranged "golf holes" (Figure 1a). They are formed in the vicinity of the substrate due to the fact that the attached blocks are shorter than the free ones. That is why the upper layer is thick enough. Increasing the length of the attached blocks (14 beads) and keeping the total length of the diblock fixed (30 beads), one can observe the morphology change in the region of interpenetration. Parallel "gullies" and "ridges" in the A layer are formed (Figure 1b). Despite a nearly symmetric composition, the bottom of the gullies comes closer to substrate in comparison with the distance from the ridges to the free surface of the film. Further increase of the relative length of the A block (18 A beads versus 12 B beads) results in transformation of the quasi-one-dimensional structure of the gullies to the structure of nearly cylindrical "stalactites" grown by B blocks (Figure 1c). The upper flat B layer is thinner than that of the previous structure because of the decrease of the B block length: it becomes comparable with the thickness of the flat A layer near the substrate (the distance between the stalactite's end and the substrate).

Further increase of the length of the A block (22 A beads versus 8 B beads) makes the stalactites thinner and longer (Figure 1d). The shortening of the B block is responsible for the decrease of their diameter, whereas the length of the stalactites increases because of disappearance of the upper flat layer. Two other "trivial" structures (not presented here) are formed by strongly asymmetric copolymers. If attached block is very short (but longer than the critical length to provide segregation), the planar bilayer is formed. In the case of very short free block, the stalactites are decoupled and form nearly spherical micelles.

The distribution of AB junctions versus vertical coordinate z is presented in the right column in Figure 1. The average fraction of the junctions, $\Delta N/N_{AB}$, is determined as the total number of the points at the distance z from the substrate, ΔN, divided by the total number of the chains (junctions) in the system, N_{AB}. The common feature of all histograms is the presence of the pronounced peak corresponding to high concentration of the junctions at the bottom side of the upper layer (for example, the regions of the ridges). To form these parts of the AB interface, the A blocks must be stretched. That is why the concentration of the junctions is high enough in these regions (the area of the interface per stretched block is small enough). On the contrary, less stretched copolymers form interfaces in the interpenetrated regions of the film (golf holes, gullies, and stalactites). That is why the concentration of the junctions is less here. The peak decreases upon shortening of the B block, especially in the case of the structure without upper flat layer (Figure 1d).

Looking at the structures, two natural questions arise. (i) What is the physical reason for the interpenetration of the A and B domains even in the case of lamellae-forming (nearly symmetric) copolymers? Or, in other words, why is the flat AB interface unstable? (ii) What is the reason for the perpendicular domain orientation?

To answer these questions, we visualized conformations of some selected chains for two structures: metastable planar bilayer (Figure 2a), which was subjected to annealing resulted

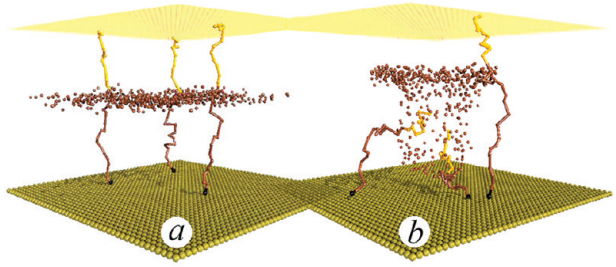

Figure 2. Conformations of the selected molecules in the planar bilayer (a) corresponding to the initial structure of the brush before annealing. The same molecules in the stalactites-like structure after annealing (the fragment of Figure 1c with one stalactite, 18_A-12_B, σ_S = 0.7, $a_{AS} = a_{BS}$ = 25) (b). Brown dots depict positions of the junctions at AB interface. The bottom and upper planes correspond to the substrate and free surface of the brush, respectively.

in the stable stalactites (Figure 2b). One can see that both blocks are strongly stretched in the planar bilayer. On the contrary, all blocks of the stalactite-like structure become less stretched except for the A block whose grafting point is located at the interface between the stalactites (right molecule in Figure 2b). However, even such simultaneous stretching (right molecule) and collapse (left and middle molecules) of A blocks results in the decrease of their elastic free energy in comparison with the case of equal stretching (see below), and the free energy of B blocks obviously gets lower after annealing. Therefore, we can state that despite an increase of the AB interfacial area, the elasticity of the chains is responsible for instability of the planar interface.

The perpendicular domain orientation in the dense brushes is also dictated by minimum stretching of the A blocks. It is well-known[27] that free ends of a homopolymer brush are located nonequidistantly from the substrate. Their distribution

dx.doi.org/10.1021/ma300890w | Macromolecules 2012, 45, 4870–4875

along z-axis is described by the black curve in Figure 1c. Nonequally stretched chains possess lower elastic free energy in comparison with equally stretched ones (well-known Alexander–de Gennes approximation[28,29]). The distribution of the diblock copolymer junctions has similar shape like in the homopolymer brush (Figure 1c). Therefore, only perpendicular domain orientation can provide broad variation in the block stretching. On the contrary, if the domains would have parallel orientation in the dense brush like in Figure 3c,d, the distribution of the junctions would be more homogeneous providing higher elastic free energy.

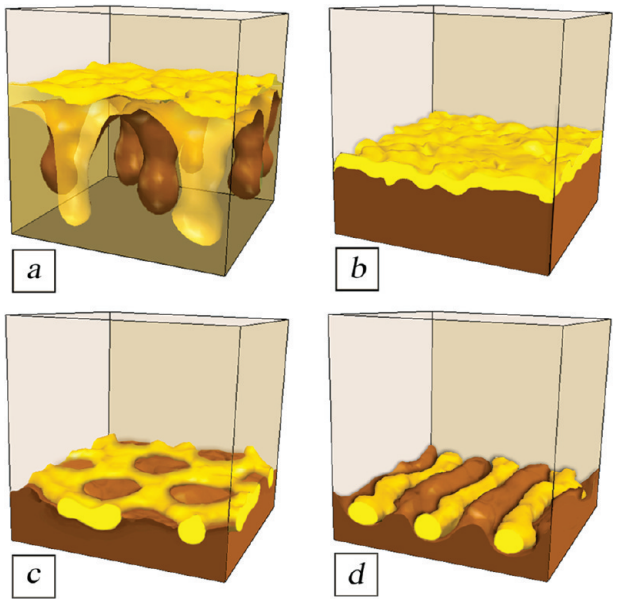

Figure 3. Effect of the "grafting" density on the morphology of the brush formed by 22_A-8_B copolymer: σ_S = 0.7 (a), 0.4 (b), 0.3 (c), and 0.2 (d). The solvent is weakly poor for both blocks, $a_{AS} = a_{BS} = 27$.

The above qualitative reasonings can be quantified. The thickness H of a densely "grafted" diblock copolymer brush homogeneously swollen in a solvent scales with the number of monomer units n as $H = q\nu n/\phi$, where q is the number of polymer chains per unit area, $\nu \sim a^3$ is an excluded volume of the monomer unit, and ϕ is the polymer volume fraction. Therefore, the free energy per chain of the bilayer structure with planar AB interface takes the form

$$\frac{F_b}{k_BT} = C_1\frac{q^2n}{\phi^2} + \frac{\gamma}{qk_BT} \quad (1)$$

where the first and the second terms are the elastic ($\sim H^2/a^2n$) and the interfacial contributions, respectively; γ is the surface tension coefficient (the energies of the substrate, free surface, and volume contribution are omitted). The numerical coefficient C_1 in the elastic free energy is higher than the corresponding coefficient of equivalent homopolymer brush because the junctions have to belong to the planar interface and A blocks must be equally stretched like in the case of the Alexander–de Gennes brush. The instability of the planar interface makes polymer chains tilted and lateral projection of the block stretching controls lateral ordering of the nanodomains. In the strong segregation regime,[27] the free energy of the nanostructures (golf holes, gullies, and stalactites) has the form

$$\frac{F_n}{k_BT} = C_2\frac{q^2n}{\phi^2} + C_3(n\gamma^2)^{1/3} \quad (2)$$

where the first term corresponds to the stretching of the blocks along z-axis and the second term includes both the elastic free energy of the lateral stretching of the blocks and the energy of AB interface. Coefficient C_2 is lower than C_1, $C_1 > C_2$, because of broader distribution of the junctions along the z-axis. Coefficient C_3 depends on composition of the copolymer, symmetry of the structure, and polymer volume fraction (it does not depend on n), $C_3 \sim 1$. Therefore, if the chains are long enough, $n \gg 1$ (or, in other words, if the brush is densely "grafted", and the parameter $q \sim 1$), then $F_b > F_n$, i.e., the nonplanar domains of the brush are more favorable. Only extremely high incompatibility between A and B units, $\gamma \sim n$, can stabilize the planar structure at $q \sim 1$.

The effect of the "grafting" density is demonstrated in Figure 3. This set of structures was obtained at parameters $a_{AS} = a_{BS} = 27$ corresponding to a weakly poor solvent for both blocks, $\chi_{AS} = \chi_{BS} = 0.572$. With the decrease of the grafting density, the stalactites-like structure (a) transforms first to a planar bilayer (b). This transition occurs at $q \sim (\gamma/n)^{1/3}$, when the first term of eq 2 becomes comparable with the second term, and the free energy F_n gets higher the energy of the planar structure, $F_b < F_n$. Then the upper layer becomes perforated and cylindrical motif appears (c). Further decrease of the grafting density leads to the decoupling of the perforated layer and formation of parallel cylindrical stripes (d). The latter structure was also obtained in refs 20 and 22 by SCFT and DPD, respectively.

All mentioned above structures were obtained for the case of $L_x = L_y = L_z = 32$. Double enlargement of lateral linear sizes of the simulation box, $L_x = L_y = 64$, $L_z = 32$, does not change morphologies of the detected microstructures. For example, stalactites-forming brush, 18_A-12_B, in a poor solvent, $a_{AS} = a_{BS} = 35$, is presented in Figure 4. The domains reveal a pronounced hexagonal order. Variation of the solvent quality from good (Figure 1c) to poor one (Figure 4a) does not change the structure significantly. This effect is due to inhomogeneous solvent distribution along the z-axis (Figure 5). In both cases the bottom part of the brush is practically nonswollen and predefines the morphology. Swelling is detectable only in the upper part or the brush. The $\phi(z)$ profile in Figure 5 is obtained for the regions of the film between the stalactites (the periphery of the Wigner–Seitz cell). Nonmonotonous behavior of the profile is due to the interface: local peak on each curve corresponds to the interface position. Accumulation of the solvent at the interface is favorable because of stronger incompatibility of A and B beads ($a_{AB} = 40$) in comparison with that of the beads and the solvent ($a_{AS} = a_{BS} = 25$ or 35).

Because of the physical attachment of the chain ends to the substrate, they are freely mobile in the xy-plane. The distribution functions of the attached ends are presented in Figure 6. The maxima of the xy-distribution (left) are achieved at the boundaries of the Wigner–Seitz cell and the fraction of the ends under the stalactites is very low (they are squeezed out by the stalactites). The vertical (z-) distribution is presented in Figure 6 (right). Most of the ends are in contact with the substrate, and only small fraction of them can reach the second layer of the cells at $z = 2$. Such distribution is allowed by moderately high value of the interaction parameter, $C_s = 5$.

dx.doi.org/10.1021/ma300890w | Macromolecules 2012, 45, 4870–4875

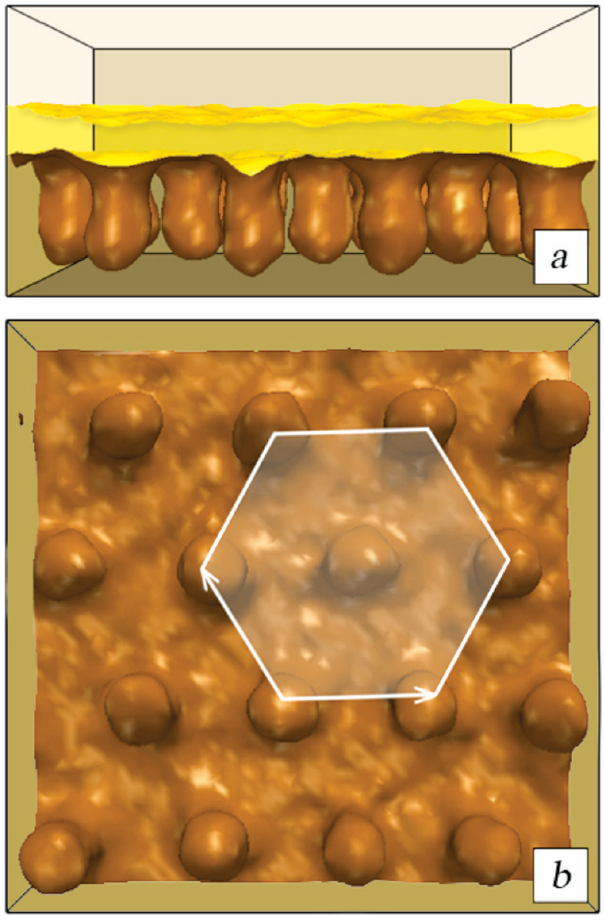

Figure 4. Side (a) and bottom (b) view of the stalactites-like structure formed by dense brush, σ_S = 0.7, of 18_A-12_B copolymer in poor solvent, $a_{AS} = a_{BS}$ = 35. The simulation box has linear sizes $L_x = L_y$ = 64 and L_z = 32.

CONCLUSION

In conclusion, we have demonstrated that dense planar brushes of physically attached diblock copolymers can reveal spatially ordered nanodomain structures perpendicularly oriented toward the substrate. Depending on composition of the copolymers, the domains can have various morphologies and sizes. Despite the perpendicular orientation, these structures do not have percolation in *z*-direction because of homogeneous boundary layers (Figure 1a–c). Therefore, similar structures of very high interfacial area can be used as templates for making efficient organic solar cells. For example, one of the possibilities to make the cells is selective removal of the components (generally by degradation) and backfilling them with donor and acceptor materials. In such devices, photons are absorbed by the donor material and excite electrons from the HOMO (highest occupied molecular orbital) to the LUMO (lowest unoccupied molecular orbital) creating excitons. The excitons travel through the donor material to the donor/acceptor (A/B) interface, where the electrons pass to the LUMO of the acceptor material breaking up the excitons into free electrons and holes. Therefore, the higher the area of the donor/acceptor (A/B) interface, the higher the concentration of the free charges. The stalactites or gullies (Figure 1b,c) are appropriate structures because of their high interfacial area. The free electrons and holes travel through the acceptor and donor materials, respectively, and arrive at corresponding electrodes (upper and bottom surfaces of the film) to create a potential gradient across the device. Therefore, if the materials are structured like in Figure 1b,c, all electrons and holes will be "active", i.e., all of them will reach the corresponding electrodes. Furthermore, due to the absence of percolation in *z*-direction, all electrons and holes will reach only "own" electrodes.

Owing to the physical attachment of the chains in the brush, one of the possibilities to experimentally realize their high stretching is the use of the Langmuir–Blodgett technique. The brush is prepared on a liquid–gas interface, where the ends of the chains are adsorbed on the interface. The film is laterally compressed until the chains begin desorption. Subsequent transfer of the compressed film on attractive solid substrate will allow fixing the structure of the film.

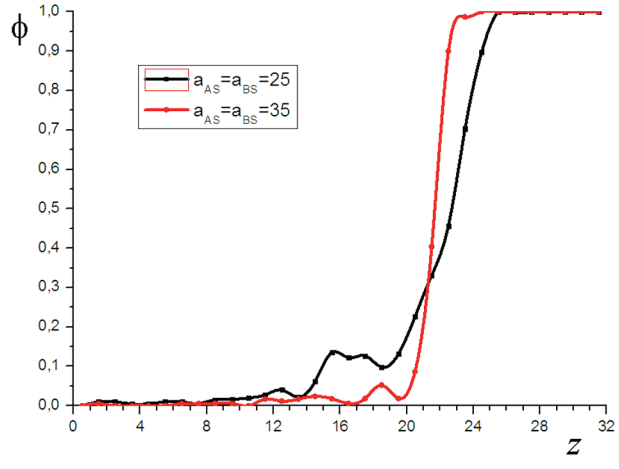

Figure 5. Good (black) and poor (red) solvent volume fraction as a function of vertical coordinate *z*. In the *xy*-plane, the profiles correspond to the regions between the stalactites (the periphery of the Wigner–Seitz cell).

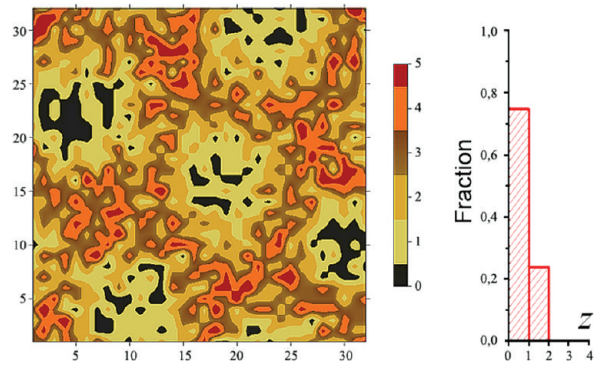

Figure 6. Lateral (left) and vertical (right) distributions of chain ends strongly attracting to the substrate. They are obtained for stalactites-like structure of the brush at 18_A-12_B, $a_{AS} = a_{BS}$ = 25, and σ_S = 0.7. The numbers of the vertical bar (left) correspond to the numbers of the ends per one 1 × 1 cell in the *xy*-plane.

AUTHOR INFORMATION

Corresponding Author

*E-mail: igor@polly.phys.msu.ru.

Notes

The authors declare no competing financial interest.

■ ACKNOWLEDGMENTS

The financial support of the Russian Foundation for Basic Research, the Ministry of Education and Science (Russian Federation), and the German Federal Ministry of Education is gratefully acknowledged. The simulations were performed on a multiteraflop supercomputer Lomonosov at Moscow State University.

■ REFERENCES

(1) Thurn-Albrecht, T.; Schotter, J.; Kästle, G. A.; Emley, N.; Shibauchi, T.; Krusin-Elbaum, L.; Guarini, K.; Black, C. T.; Tuominen, M. T.; Russell, T. P. *Science* **2000**, *290*, 2126−2129.
(2) Topham, P. D.; Parnell, A. J.; Hiorns, R. C. *J. Polym. Sci., Part B* **2011**, *49*, 1131−1156.
(3) Turner, M. S.; Johner, A.; Joanny, J.-F. *J. Phys. I (Paris)* **1995**, *5*, 917−932.
(4) Potemkin, I. I. *Macromolecules* **2004**, *37*, 3505−3509.
(5) Ryu, D. Y.; Wang, J.-Y.; Lavery, K. A.; Drockenmuller, E.; Satija, S. K.; Hawker, C. J.; Russell, T. P. *Macromolecules* **2007**, *40*, 4296−4300.
(6) Busch, P.; Posselt, D.; Smilgies, D.-M.; Rheinländer, B.; Kremer, F.; Papadakis, C. M. *Macromolecules* **2003**, *36*, 8717−8727.
(7) Potemkin, I. I.; Busch, P.; Smilgies, D.-M.; Posselt, D.; Papadakis, C. M. *Macromol. Rapid Commun.* **2007**, *28*, 579−584.
(8) Kim, S. O.; Solak, H. H.; Stoykovich, M. P.; Ferrier, N. J.; de Pablo, J. J.; Nealey, P. F. *Nature* **2003**, *424*, 411−414.
(9) Stoykovich, M. P.; Muller, M.; Kim, S. O.; Solak, H. H.; Edwards, E. W.; de Pablo, J. J.; Nealey, P. F. *Science* **2005**, *308*, 1442−1446.
(10) Kriksin, Yu. A.; Neratova, I. V.; Khalatur, P. G.; Khokhlov, A. R. *Chem. Phys. Lett.* **2010**, *492*, 103−108.
(11) Kriksin, Yu. A.; Khalatur, P. G.; Neratova, I. V.; Khokhlov, A. R.; Tsarkova, L. A. *J. Phys. Chem. C* **2011**, *115*, 25185−25200.
(12) Albrecht, K.; Mourran, A.; Zhu, X.; Markkula, T.; Groll, J.; Beginn, U.; de Jeu, W. H.; Möller, M. *Macromolecules* **2008**, *41*, 1728−1738.
(13) Potemkin, I. I.; Bodrova, A. S. *Macromolecules* **2009**, *42*, 2817−2825.
(14) Morkved, T. L.; Lu, M.; Urbas, A. M.; Ehrichs, E. E.; Jaeger, H. M.; Mansky, P.; Russell, T. P. *Science* **1996**, *273*, 931−933.
(15) Olszowka, V.; Hund, M.; Kuntermann, V.; Scherdel, S.; Tsarkova, L.; Böker, A.; Krausch, G. *Soft Matter* **2006**, *2*, 1089−1094.
(16) Zhulina, E. B.; Singh, C.; Balazs, A. C. *Macromolecules* **1996**, *29*, 8254−8259.
(17) Yin, Y.; Sun, P.; Li, B.; Chen, T.; Jin, Q.; Ding, D.; Shi, A.-C. *Macromolecules* **2007**, *40*, 5161−5170.
(18) Tomlinson, M. R.; Genzer, J. *Polymer* **2008**, *49*, 4837−4845.
(19) Wang, J.; Müller, M. *Macromolecules* **2009**, *42*, 2251−2264.
(20) Matsen, M. W.; Griffiths, G. H. *Eur. Phys. J. E* **2009**, *29*, 219−227.
(21) O'Driscoll, B. M. D.; Griffiths, G. H.; Matsen, M. W.; Hamley, I. W. *Macromolecules* **2011**, *44*, 8527−8536.
(22) Guskova, O. A.; Seidel, C. *Macromolecules* **2011**, *44*, 671−682.
(23) Hoogerbrugge, P. J.; Koelman, J. M. V. A. *Europhys. Lett.* **1992**, *19*, 155−160.
(24) Koelman, J. M. V. A.; Hoogerbrugge, P. J. *Europhys. Lett.* **1993**, *21*, 363−368.
(25) Groot, D.; Warren, P. B. *J. Chem. Phys.* **1997**, *107*, 4423−4435.
(26) Pagonabarraga, I.; Hagen, M. H. J.; Frenkel, D. *Europhys. Lett.* **1998**, *42*, 377−382.
(27) Semenov, A. N. *Sov. Phys. JETP* **1985**, *61*, 733−742.
(28) Alexander, S. *J. Phys. (Paris)* **1977**, *38*, 983−987.
(29) de Gennes, P. G. *Macromolecules* **1980**, *13*, 1069−1075.